# Research on the drying Mechanism of Astragali Radix during Processing

**Jie Peng**
Jinan University
**Meng-Mei Wu**
Jinan University
**Li-Fang Ye**
Jinan University
**Meng-Hua Wu**
Jinan University
**Zhi-Guo Ma**
Jinan University
**Hui Cao**
Jinan university
**Ying Zhang** ( zhangying@jnu.edu.cn )
Jinan university

**Research**

**Keywords:** Traditional Chinese Medicine, Astragali Radix pieces, Drying kinetics, LF-NMR, MRI, Texture analyzer

**Posted Date:** October 12th, 2021

**DOI:** https://doi.org/10.21203/rs.3.rs-958988/v1

# Research on the drying mechanism of Astragali Radix during processing

Jie Peng[1,2], Meng-Mei Wu[1], Li-Fang Ye[1], Meng-Hua Wu[1,2], Zhi-Guo Ma[1,3], Hui Cao[1,3†*], Ying Zhang[1,2†*]

*Correspondence: kovhuicao@aliyun.com; zhangying@jnu.edu.cn

†Hui Cao and Ying Zhang contributed equally to this study

[1] Research Center for TCM of Lingnan (Southern China), Jinan University, Guangzhou, P. R. China

Full list of author information is available at the end of the article

## Abstract

**Background:** Astragali Radix (Huangqi) is an important Chinese herbal medicine that is always processed into pieces for clinical use. There are many operations required after harvesting, among which drying of AR pieces is a key step. Unfortunately, research on the drying mechanism is still limited.

**Methods:** Low-field nuclear magnetic resonance (LF-NMR) and magnetic resonance imaging (MRI) techniques were applied to study the water status and water distribution during the drying process. The contents of bioactive ingredients and texture changes were measured by HPLC and texture analyzer, respectively.

**Results:** During the drying process, the moisture content first decreased rapidly. After a particular time, the moisture content decreased slowly, and the equilibrium value was reached. The trends for changes in flavonoid glycoside and flavonoid aglycone contents

in AR pieces were entirely opposite. The relaxation times $T_{22}$ and $T_{23}$ and the peak areas $A_{22}$ and $A_{Total}$ decreased significantly during drying. In addition, the intensity of the water signal decreased from the surface to the interior. The textural parameters hardness, adhesion and fracturability increased without an apparent change in springiness. The parameters of LF-NMR and the texture analyzer were correlated with water content.

**Conclusions:** This study indicated that HPLC, LF-NMR, MRI and texture analyzers provide a scientific basis for elucidating the principles for drying of AR pieces. The method is useful and shows potential for popularization and application; accordingly, it can easily be extended to other radix and/or rhizoma Traditional Chinese Medicinal materials.

**Keywords:** Traditional Chinese Medicine, Astragali Radix pieces, Drying kinetics, LF-NMR, MRI, Texture analyzer

## Background

Processing, *Paozhi* in Chinese, is a unique Chinese pharmaceutical technique with a long history of facilitating the use of Chinese herbal medicines for specific clinical needs based on Traditional Chinese Medicine (TCM) theory [1]. The Chinese medicine Yinpian is an important product of processing and is directly suitable for clinical use [2]. Most Yinpian needs to remain dry before use, with the exception of a small number that can be used when they are fresh [3]. The dried medicinal materials from production have impurities removed, they are cleansed, moistened, cut, and dried, and then different decoction pieces are made accordingly. Among these procedures, drying is the

crucial step in which water inside medicinal materials is removed in time to facilitate storage [4].

Astragali Radix (Huangqi in Chinese) originated from the dried root of *Astragalus membranaceus* (Fisch.) Bge. var. *mongholicus* (Bge.) Hsiao or *Astragalus membranaceus* (Fisch.) Bge. have been used as Traditional Chinese Medicines (TCMs) for more than 2,000 years [5]. Astragali Radix (AR) can tonify the middle-jiao and replenish qi, solidify the surface and promote diuresis, dispel sepsis and renew muscle [6]. Modern research shows that AR has many biological functions, such as vasodilation [7], antioxidant activity [8, 9], immunomodulation [10, 11], antiaging activity [12, 13], and antitumor activity [14]. The process of producing AR decoction pieces is “remove impurities, separate size, cleanse, moisten, cut thick pieces and dry [15].” At present, research reports on drying AR pieces are shallow and mainly use appearance, shape and other indicators to purse an optimum drying process. There is a lack of research on the mechanism for the drying process. It is impossible to guarantee the quality of prepared pieces after the drying process or to optimize process parameters. At the same time, there are many reports on drying mechanisms for fruits, vegetables and seafoods, such as strawberries [16], garlic [17], carrots [18] and abalone [19]. The above studies typically use combinations of multiple technologies to monitor changes in physical properties that occur during drying. Among them, low field nuclear magnetic resonance (LF-NMR), magnetic resonance imaging (MRI) and texture analyzers have obvious advantages in detecting material texture changes and migration, distribution and transformation of water.

LF-NMR and MRI are powerful tools for analyzing water states and distributions in food matrices due to their sensitivity, fast analysis speed, and low cost, and they are also non-invasive and non-destructive [20]. The abundance of water in moistened TCMs ensures strong signals in NMR relaxometry/MRI, which makes them ideal samples for these methods. The transverse relaxation time ($T_2$) primarily provides information on water status and the binding of water in the food matrix, while MRI indicates the spatial distribution of water and changes during processing [21]. Additionally, a texture analyzer is a multifunctional probe of physical properties. Through a variety of test modes, such as compression, puncture, shearing and stretching, hardness, adhesion, elasticity, cohesiveness and other physical property parameters are characterized, and the instruments are objective, sensitive, and accurate [22].

The main objective of this study is to evaluate the drying characteristics of AR pieces at different drying temperatures and then select the optimum drying temperature for the bioactive ingredients present. The state, distribution, migration and transformation of water in drying AR pieces will be determined using LF-NMR and MRI. The results from the drying curves and LF-NMR data will clarify the relationship between moisture loss and the movement of water in different states during drying of AR pieces. The changes in the physical properties of AR pieces during drying will also be evaluated. The results will provide a theoretical basis for optimization of the drying process and improvement in AR quality.

## Materials and methods

## Materials

Astragali Radix was collected from Min County (Gansu Province, China) in September 2020 and was identified as the dried root of *Astragalus membranaceus* (Fisch.) Bge var. *mongholicus* (Bge.) Hsiao by Dr. Ying Zhang at the Research Center for Traditional Chinese Medicine of Lingnan (Southern China) of Jinan University. The medicinal specimens were deposited in the specimen cabinet of the Research Center for TCM of Lingnan (Southern China), Jinan University.

## Chemical and standards

HPLC-grade methanol and acetonitrile were purchased from Thermo Fisher Scientific (Fair Lawn, NJ, USA). HPLC-grade phosphoric acid was obtained from Shanghai Macklin Biochemical Co., Ltd. (Shanghai, China). Purified water used for the chromatographic mobile phase was purchased from China Resources Yibao Beverage (China) (Guangzhou, China). Other reagent solutions were of analytical grade (Guangdong Guanghua Sci-Tech Co., Ltd., Shantou, China).

The standard substances calycosin-7-O-beta-D-glucoside (batch number: RFS-M02001902019), ononin (batch number: RFS-M01301904002), calycosin (batch number: RFS-M02101903026), and formononetin (batch number: RFS-C01811812016) were purchased from Chengdu Herbpurify Co., Ltd. (Chengdu, China). The purity of all reference compounds was >98%, as determined by normalization of the peak areas detected by HPLC.

**Drying experiments with AR pieces**

The raw AR pieces were homemade in the laboratory: 600 g of AR was fully moistened in distilled water, and then AR was cut into pieces with diameters of 2–4 mm. The above pieces were evenly divided into three parts, placed on a drying tray in a single layer, dried in an electric heating blast oven (Tianjin City Taisite Instrument Co., Ltd., 101-2AB, Tianjin, China) at temperatures of 70°C, 80°C, and 90°C, and the layer thickness was approximately 4–8 mm. The moisture content was measured by weighing the sample every 30 min until the weight became constant. The drying process stopped when the weight difference between two adjacent time points was within 1% of the total weight, which is considered to be a safe level for long-term storage.

**Moisture content, moisture ratio and drying rate**

In this section, two parameters for drying characteristics, moisture ratio (MR) and drying rate (DR), were measured. First, the moisture content (g/g, d.b.) of AR pieces were calculated based on Equation (1):

$$MC_t = (m_t - m_e)/m_e \quad (1)$$

where $MC_t$ is the moisture content of AR pieces dried for time $t$, $m_t$ is the mass (g) of AR pieces at time $t$, and $m_e$ is the mass (g) of the dry basis.

The moisture ratio (MR) and drying rate (DR) can be expressed as follows [23]:

$$MR = (MC_t - MC_e)/(MC_0 - MC_e) \quad (2)$$

$$DR = (MC_t - MC_{t+\Delta t})/\Delta t \quad (3)$$

where $MC_0$ and $MC_e$ are the initial moisture content (g/g, d.b.) and the final

equilibrium moisture content of AR pieces, and $MC_t$ and $MC_{t+\Delta t}$ are the moisture content (g/g, d.b.) at times $t$ and $t + \Delta t$, respectively. $MC_e$ can be assumed to be zero when compared with $MC_0$.

**Determination of bioactive ingredient content by HPLC**

The AR pieces dried for different times were smashed and filtered through a 65 mesh sieve. Extracts were prepared according to the procedure described in the *Chinese Pharmacopoeia (2020 edition)* [15]. Chromatographic separation was carried out using an Agilent 1260 liquid chromatography system (Santa Clara, USA) equipped with a diode array detector (190–400 nm), a quaternary solvent delivery system, a column temperature controller, and an autosampler. Chromatographic data were recorded and processed with Agilent chromatographic workstation software. Separation was performed on a COSMOSIL C18 column (5C18-MS-II Packed Column, 4.6 mm I.D. × 250 mm, 5μm, Code 38020-41). The mobile phase was prepared from 0.5% aqueous phosphoric acid solution (A) and acetonitrile (B). The gradient program for HPLC was as follows: 0–5 min, linear gradient 20–35% B; 5–15 min, linear gradient 35–50% B; 15–30 min, linear gradient 50–65% B; and post run (5 min) at a flow rate of 1 mL/min. The injection volume was 10 μL, and the column temperature was maintained at 35°C. Signal monitoring was performed at 250 nm. Four reference samples were accurately weighed and put in a 5-mL volumetric flask and dissolved in methanol to form standard stock solutions. Appropriate volumes of stock solutions were mixed and diluted to form a mixed standard solution, in which the concentrations of calycosin-7-O-beta-D-

glucoside, ononin, calycosin and formononetin were 1.294, 0.874, 0.372 and 1.098 mg/mL, respectively.

**LF-NMR and MRI analysis**

Relaxation ($T_2$) analysis was performed on a MesoMR23-060H-I NMR analyzer (Suzhou Niumag Analytical Instrument Co., Ltd.) with a 0.5 T permanent magnet and a 60 mm diameter radio frequency, corresponding to a proton resonance frequency of 21 MHz at 32 ± 0.01°C with 90° and 180° pulses of 10 μs and 19.04 μs. The samples were equilibrated to room temperature for measurements of transverse relaxation time $T_2$. Measurement conditions were as follows: TW (time waiting) = 5,000 ms, TE (time echo) = 0.30 MS, NECH (number of echoes) = 8,000, SW (signal receiving bandwidth) = 100 kHz, NS (number of scans) = 4. NMR analysis software (Suzhou Niumag Analytical Instrument Co., Ltd.) and Carr–Purcell–Meiboom–Gill (CPMG) pulse sequences were used to collect the relaxation signals. Simultaneous iterative reconstruction was performed at 100,000 for inversion to obtain the relaxation map of the samples.

Magnetic resonance imaging was performed with the same LF-NMR analyzer and spin-echo sequence. The samples were placed in the center of the radio frequency coil, the signal was collected, and $T_2$-weighted images were obtained. Image processing software was used to map and process the MRI image. The main parameters were as follows: TE (time echo) = 20 ms, TR (time repetition) = 1000 ms, flip angle = 90º, refocus flip angle = 180º, averages = 4, read size = 256, phase size = 192, RG = 20 dB,

PRG was high, FOV = 100 × 100 mm, slice width = 2.0 mm, slice gap = 1.0 mm and slices = 5.

**Measurement of texture parameters**

The texture profiles of the samples were determined only in the center part by a texture analyzer (CT3, Brookfield Engineering Laboratory Instrument Co., Ltd., Guangzhou, China). Under the compression model, the probe was TA9 (needle, 1.0 mm in diameter, 43 mm in length). The parameters were as follows: test speed of 1 mm/s, return speed of 1 mm/s, trigger point load of 5 g, puncture depth of 6 mm, and data frequency of 50 points/sec, with a load cell of 10000 g. Textural data were analyzed automatically by texture loader software (Brookfield Engineering Laboratory Instrument Co., Ltd., Guangzhou, China). The typical textural variables measured for AR pieces were hardness, adhesion, springiness, and fracturability.

**Statistical analysis**

All data were input into EXCEL software and analyzed by Statistical Package for the Social Sciences software, version 24 (SPSS, Chicago, IL, USA). One-way analysis of variance (ANOVA) was used to determine whether differences between mean values were significant. The statistical significance of the differences was tested at a probability level of 5% ($p < 0.05$). Plots were produced using Origin 2018 64 Bit software (Origin Laboratory, Northampton, MA, USA) and GraphPad Prism v.8.0 software (San Diego, CA, USA).

## Results

### Drying characteristics

The drying characteristics curves for AR pieces during hot-air drying at different temperatures are shown in Figure 1. The drying times required to reach the equilibrium moisture content for AR were 180, 150, and 120 min at 70ºC, 80ºC, and 90ºC, respectively. Figure 1a shows that the higher the temperature was, the shorter the time needed to reach the same moisture content. Compared with the drying time required at 70ºC, those at 80ºC and 90ºC were 16.67% and 33.33% less, respectively. Moisture ratio (MR) curves were reduced exponentially with drying time (Fig. 1a). Curves that exhibited steeper slopes had higher drying rates. As shown in Figure 1b, the curve for drying at 90ºC exhibited the steepest slope, followed by the curves for 80ºC and 70ºC. Although the MR of the 90ºC sample declined faster than that of the 70ºC sample, it was not significantly different from that of the 80ºC sample. However, the 70ºC sample required a longer time than the 90ºC or 80ºC samples to achieve the final moisture content.

The curves for drying rate are shown in Figure 1c. When the drying time was 0.5 h, the drying efficiencies for the three different temperatures reached their maximum values. Before 1.5 h, there was considerable water in the AR pieces, and higher temperatures led to more water loss per unit time. The drying rate curves were arranged according to temperature from high to a low. At 1.5 h, the drying rates for the three different temperatures were almost the same and had reached the equilibrium state.

After 1.5 h, the drying curves were completely reversed and were inversely proportional to temperature.

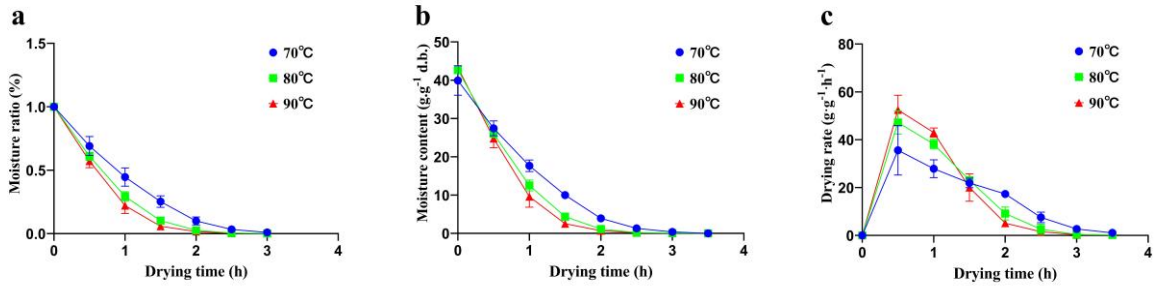


**Fig. 1** Drying characteristics of AR pieces. **a** Moisture ratio. **b** Moisture content. **c** Drying rate. Data are represented as the mean ± SD of three independent experiments (n = 3).

## Dynamic changes of flavonoids in the thermal drying process

The contents of calycosin-7-O-beta-D-glucoside (CG), ononin, calycosin and formononetin, the four major flavonoids of AR, were measured. The total flavonoid content was determined by summing the content of each of the four flavonoids. The results are shown in Table1. The contents of CG and ononin ranged from 0.65 ± 0.03 mg/g to 0.84 ± 0.09 mg/g and from 0.14 ± 0.02 mg/g to 0.17 ± 0.01 mg/g, respectively. The highest content was seen after drying at 80°C, and the lowest resulted after drying at 70°C. As the drying temperature was increased, the total flavonoid content gradually increased, but there was no significant difference among the three temperatures. At present, CG is used as an index for flavonoids in the evaluation of AR quality in the *Chinese Pharmacopoeia (2020 edition)*; the higher its content is, the greater the medicinal value of AR. By considering the contents of CG and total flavonoids, it was concluded that 80°C was the optimal drying temperature in this work, and follow-up

tests will also be conducted based on 80°C. During drying at 80°C, the trends for changes in the contents of flavonoid glycoside and flavonoid aglycone in AR pieces were completely opposite: the contents of CG and ononin were decreased at the end of the drying process, while those of calycosin and formononetin were ultimately increased (Fig. 2).

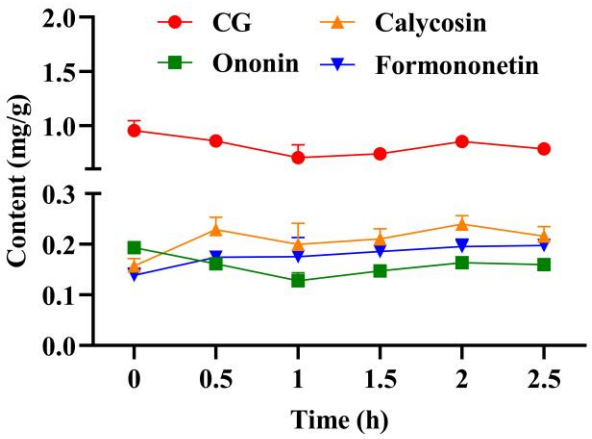


**Fig. 2** Contents of CG, calycosin, ononin and formononetin in AR pieces during drying at 80°C. Data are represented as the mean ± SD of three independent experiments (n = 3).

## LF-NMR moisture state analysis

The $T_2$ relaxation curves (Fig. 3a) show that three water populations were present in the drying AR pieces and they exhibit various relaxation times; these are defined as $T_{21}$ (0–10 ms), $T_{22}$ (10–100 ms) and $T_{23}$ (100–1000 ms), which correspond to bound, immobile and free water, respectively. Normalized by the mass of the sample, the contents of bound water ($A_{21}$), immobile water ($A_{22}$), free water ($A_{23}$) and total water ($A_{Total}$) during drying are shown in Table 2. Significant changes ($p < 0.05$) were observed for all moisture content. For moistened AR pieces, $A_{23}$, $A_{22}$, and $A_{21}$ accounted for 1.47%,

97.89%, and 0.64% of the total water content, respectively. The values of $A_{total}$ and $A_{22}$ declined rapidly for all drying treatments until equilibrium was reached. That is, the content of water present in the tissue spaces decreased during all drying processes. However, the values of $A_{21}$ tended to increase originally and then decrease, but they tended to decline gradually overall (Fig. 3b).

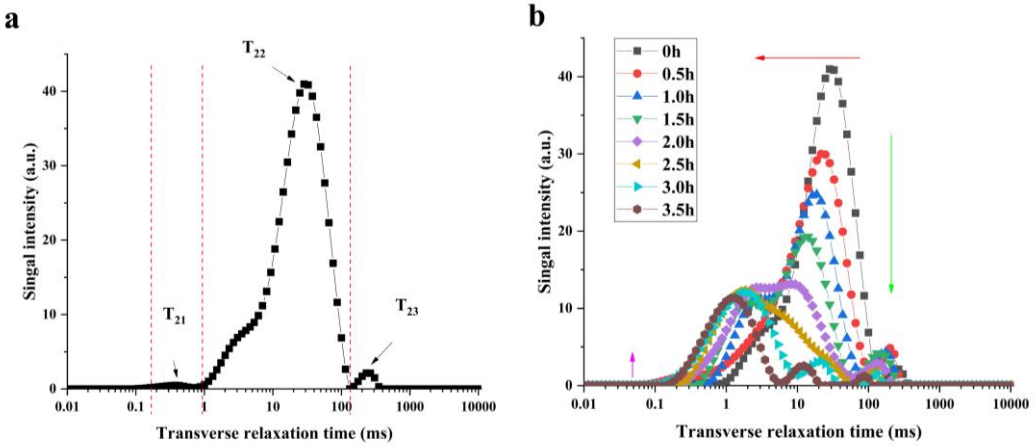


**Fig. 3** Transverse relaxation time ($T_2$) curves for AR pieces during drying. **a** Sample not dried. **b** Samples after different drying times.

## MRI water migration analysis

Figure 4 shows $T_2$-weighted MRI images of AR pieces dried at 80°C. The blue color indicates a low relaxation signal, and the red color indicates a high relaxation signal. With extension of drying times, the MRI images of AR pieces gradually became darker; the proton density gradually decreased and the signal color finally became light blue, indicating that the moisture content of AR pieces gradually decreased. The $T_2$-weighted images of AR at 2.5 h showed that there was still some water in the phelloderm and xylem of the AR, and it had nearly disappeared at 3 h. The MRI images show that the

relaxation signals for protons outside of the AR pieces weakened at first, indicating that free water was mostly distributed outside the AR pieces, while immobile water and bound water were primarily distributed inside the AR pieces.

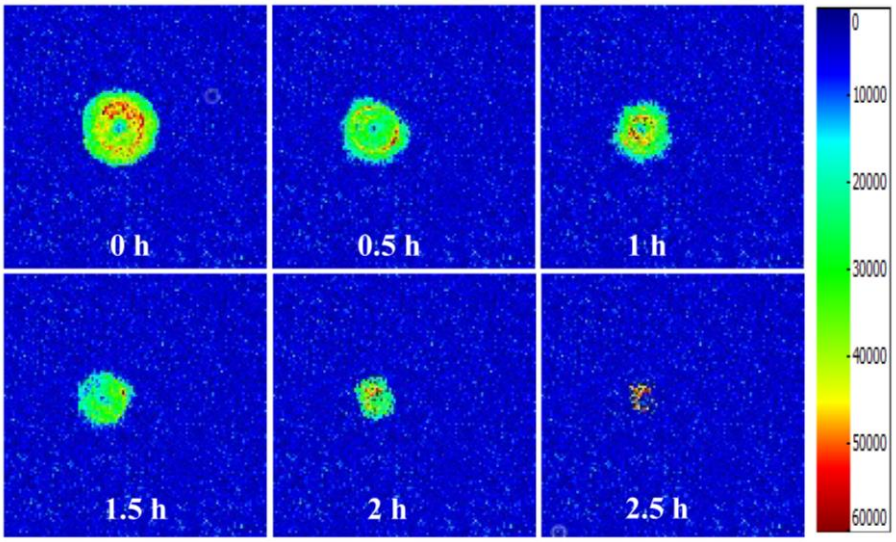


**Fig. 4** $T_2$-weighted MRI images of AR pieces during drying at 80°C.

**Texture analysis**

Table 3 shows the textural parameters for hardness, adhesion, springiness, and fracturability of AR pieces during drying. Hardness, adhesion and fracturability increased significantly with the extension of drying time, especially during the final drying period. The hardness value increased from 686.33 ± 23.18 g to 2656.67 ± 43.84 g, the adhesion value increased from 160.00 ± 5.57 g to 1163.67 ± 29.91 g, and the fracturability value increased from 189.67 ± 69.29 g to 520.00 ± 128.85 g when drying ended (2.5 h).

Figure 5 contains the load curves for AR pieces during drying. Figure 5a shows clearly that the hardness of AR increased tremendously during drying. From 0 h to 1.0

h, the hardness change was not yet obvious, but the height of the curve doubled from 1.0 h to 2.5 h and doubled again from 2.5 to 3.5 h. The hardness of AR gradually increased and finally achieved balance during the drying process. Figure 5b shows a complete test. From the figure, we know key information such as hardness, fracturability, and adhesion. Characteristic textural parameters were measured and defined as follows: hardness was the maximum force of the first bite; adhesion was the negative force area for the first bite; fracturability was the force at the first peak; springiness was the distance of the detected height during the second compression divided by the original compression distance. The measurement curve in Figure 5b that appeared in the negative ordinate area resulted from AR squeezing of the puncture needle during the return stroke after the puncture was completed. At the same time, the curve was not completely smooth (Fig. 6). Based on its anatomy, Astragali Radix can be roughly divided into three parts: phellem, phelloderm and xylem. Due to the different functions of the three tissue structures, the types and arrangements of the cells within them are different, and this resulted in different hardness values and ultimately in unsmooth hardness curves.

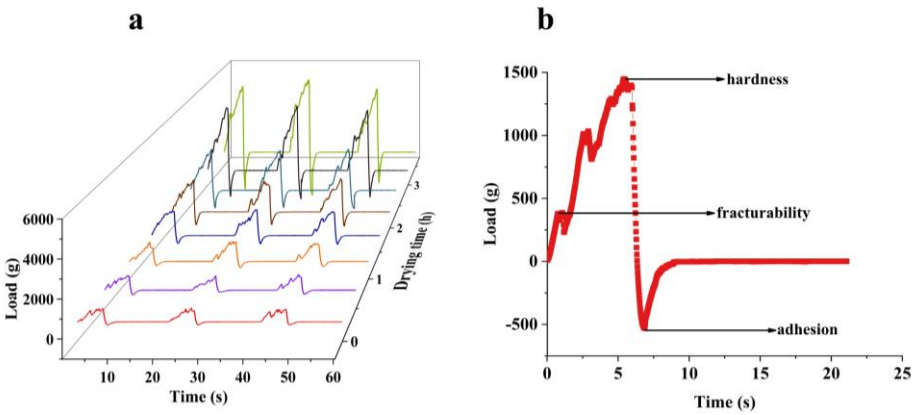


**Fig. 5** Load curves for AR pieces during drying. **a** Samples after different drying times. **b** One complete test.

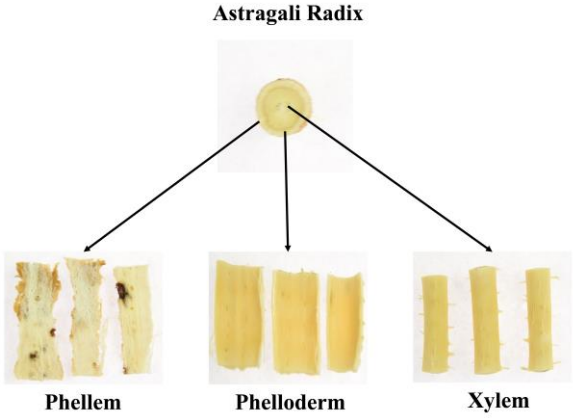


**Fig. 6** Anatomy of Astragali Radix.

## Correlation analysis of moisture content, textural parameters, and LF-NMR data

To identify the relationships among moisture content, textural parameters, and LF-NMR data, we used correlation analysis to analyze moisture content, the four texture parameters (hardness, adhesion, springiness, and fracturability), and the seven LF-NMR parameters ($T_{21}$, $T_{22}$, $T_{23}$, $A_{21}$/g, $A_{22}$/g, $A_{23}$/g and $A_{Total}$/g) (Table 4). The parameters $T_{22}$, $T_{23}$, $A_{22}$/g, and $A_{Total}$/g exhibited highly positive correlations, with

correlation coefficients between 0.798 and 0.972; the two exceptions were $A_{23}$/g ($r$ = 0.355) and springiness ($r$ = 0.310). It was clear that $A_{Total}$/g had an extremely strong correlation with MC ($r$ = 0.972). The remaining LF-NMR factors, $T_{21}$, $A_{21}$/g and the three main texture elements (hardness, adhesion and fracturability), were highly negatively intercorrelated.

## Discussion

The drying characteristics of products are influenced by various factors, such as the drying method, thickness of the product, drying temperature, and drying time [24]. Irrespective of drying temperature, the drying processes for AR pieces remained mainly in the falling-rate stage; this indicated that diffusion was limited by internal water transfer [25], since drying efficiency depends on the nature of the material and the difficulty of capillary diffusion [26]. These results agreed with those for other biological materials [27-29]. The whole process of drying AR pieces was mainly characterized by increasing speed and decreasing time periods, and there was almost no constant time period, which was consistent with many previous studies [30, 31].

Changes in chemical composition are an important index for evaluating the quality of Chinese herbal medicines [32]. The metabolic efficiencies for digestion of flavonoid glycosides and flavonoid aglycones in the human small intestine are different [33], so monitoring the changes in index components during drying of a TCM is of great significance in controlling the quality of TCM decoction pieces. The results obtained in the present study showed that high-temperature drying treatments led to significant

dynamic changes in flavonoid contents in AR pieces. It may be that flavonoid glycosides in AR pieces showed a certain degree of thermal instability, such that thermal treatment led to degradation of AR flavonoid glycosides. Similar phenomena have been reported for secondary metabolites in other medicinal or food materials, such as celery, onion and black beans (*Phaseolus vulgaris* L). [33-35].

To investigate the internal moisture contents of the AR pieces during drying, their $T_2$ values were monitored using LF-NMR [20]. Higher $T_2$ relaxation times are consistent with weaker binding or greater degrees of freedom for hydrogen. $T_{21}$ relaxation is ascribed to water molecules (hydration monolayer) bound by strong H-bonds, which are associated with the water contained in cell walls. Region $T_{22}$ represents the water molecules (multilayer water) strongly bound to the monolayer, which involves water contained in the cytoplasm and extracellular space [36]. Similar findings were evident in other studies related to TCMs, such as for *Gastrodia elata Blume* with infrared-forced circulation drying [37].

As the drying time increased, the $T_2$ relaxation time decreased significantly and moved to the left, suggesting a lower level of water mobility. The values of $T_{22}$ and $T_{23}$ were greater than those of $T_{21}$, and this suggested that the water lost from AR pieces came mainly from free and immobile water. By observing the proportions of the three types of water, we can conclude that the internal moisture was mainly due to free water and that most of the moistened AR pieces did not contain free water but had immobile water due to processing at the site of origin. Both quantitative and qualitative changes took place during drying, and immobile water evaporated considerably during drying

and was also transformed into bound water. The correlation values suggested that it might be possible to assess weight loss by using LF-NMR to monitor the AR drying process in a rapid and nondestructive way.

MRI is a technique capable of providing information on the water content or mobility of water molecules. MRI is useful for real-time, noninvasive, and quantitative measurements, and it detects the spin–spin relaxation times ($T_2$) of water protons, which provide information on water mobility. A shorter $T_2$ indicates less mobility of the water molecules [38]. A brighter MRI image represents a stronger resonance signal and a higher proton density. Conversely, weaker signals indicate lower proton densities [39]. The green color of MRI in all AR samples was shifted toward blue with the extension of drying time. The decreased moisture content of AR was directly related to the drying time, and the signal intensities of the $T_2$-weighted images changed in response to significant changes in water distribution in AR during drying. Intracellular moisture exhibited a lower migration rate than surface moisture. In other words, the signal intensities decreased gradually in the areas close to the surface and most exposed to drying. This indicated that hot-air drying was an inhomogeneous drying process, while microwave freeze drying was a uniform drying process [40]. MRI allows visualization of the drying status of AR during drying.

Texture, particularly hardness, is one of the most important parameters used to judge the sensory quality of dried TCMs [41]. The texture of a plant material depends on complex interactions between different levels of the structural organization, from the molecular level (cell wall polymers) up to the organization of cells in different

tissues and organs [42]. After drying, the interiors of the AR pieces were denser than those of the moistened pieces. Fibers are elongated cells with tapering ends and very thick, heavily lignified cell walls. Fiber cells are dead at maturity and function as support tissues in plant stems and roots [43]. Due to the highly fibrous nature of the samples, adhesion gradually increased. The dried AR samples were more fragile than the moistened samples, which may explain the increased fracturability. However, the springiness did not change significantly in our study during dehydration. The principal reason for the increased hardness was probably the substantial removal of water during drying; this induced structural changes in AR cells or tissue and created a compact microstructure and greater hardness and fracturability.

Correlation analysis showed that there was a certain correlation between moisture content, the four texture parameters, and the seven LF-NMR parameters. Therefore, it is feasible to use total signal amplitude to predict moisture content. It has also been demonstrated that LF-NMR/MRI and texture analyzers are convenient technologies for clarifying the mechanism for drying during the process.

## Conclusion

In this study, three equations and four instruments were used together to study the mechanism for drying of AR pieces, quantitative and visual results were achieved, and there were certain correlations between parameters. This makes it possible to guarantee the quality of prepared pieces after the drying process or to optimize process parameters. Accordingly, the method can easily be extended to other radix and/or rhizoma

Traditional Chinese Medicinal materials.

## Abbreviations

TCM: Traditional Chinese Medicine; LF-NMR: Low-field nuclear magnetic resonance; MRI: Magnetic resonance imaging; MR: Moisture ratio; DR: Drying rate; MC: Moisture content; HPLC: High-performance liquid chromatography; CG: Calycosin-7-O-beta-D-glucoside.


## Acknowledgments

Not applicable.


## Authors' contributions

JP compiled all data, discussed the data with all other authors, wrote and edited the manuscript. MMW and LFY helped to visualize data with software. MHW revised the manuscript. ZGM and YZ designed and supervised this work. HC read and approved the final manuscript. All authors read and approved the final manuscript.


## Funding

This work was supported by the National Key Research and Development Project of China under Grant (No. 2019YFC17115000), the Project supported by the National Natural Science Foundation of China (No. 82074015), the Guangdong Basic and Applied Basic Research Foundation (No. 2020A151501577).

## Availability of data and materials

All data used to support the findings of this study are available from the author upon reasonable request.

## Ethics approval and consent to participate

Not applicable.

## Consent for publication

All authors consented to the publication of this manuscript.

## Competing interests

The authors declare that they have no competing interests.

## Author details

[1] Research Center for TCM of Lingnan (Southern China), Jinan University, Guangzhou, P. R. China.

[2] National Engineering Research Center for Modernization of Traditional Chinese Medicine Lingnan Resources Branch, Guangzhou, P. R. China.

[3] Guangdong Key Laboratory of Traditional Chinese Medicine Information Technology, Guangzhou, P. R. China.

1. Sheridan H, Kopp B, Krenn L et al. Traditional Chinese herbal medicine

preparation: Invoking the butterfly effect. Science. 2015; 350: S64-S66.

2. Zhao ZZ, Liang ZT, Chan K et al. A Unique Issue in the Standardization of Chinese Materia Medica: Processing. Planta Medica. 2010; 76: 1975-1986.

3. Xu W, Li J, Song F et al. Research Progress of the Drying Technology of Chinese Herbal Medicine. Medicinal Plant. 2014; 5: 8-11.

4. Oliveira WP, Bott RF, Souza CRF. Manufacture of standardized dried extracts from medicinal Brazilian plants. Dry Technol. 2006; 24: 523-533.

5. Bi YQ, Bao HY, Zhang CH et al. Quality Control of Radix Astragali (The Root of Astragalus membranaceus var. mongholicus) Along Its Value Chains. Front Pharmacol. 2020; 11: 14.

6. Shi H. Shen Nong Ben Cao Jing Beijing: People's Medical Publishing House; 1982.

7. Wu XL, Wang YY, Cheng J et al. Calcium channel blocking activity of calycosin, a major active component of Astragali Radix, on rat aorta. Acta Pharmacol Sin. 2006; 27: 1007-1012.

8. Xiao QL, Bai XL, Gao P et al. Application of Convolutional Neural Network-Based Feature Extraction and Data Fusion for Geographical Origin Identification of Radix Astragali by Visible/Short-Wave Near-Infrared and Near Infrared Hyperspectral Imaging. Sensors. 2020; 20: 14.

9. Siwicka D, Skopinska-Rozewska E, Bodera P. Immunotropic and anti-tumor effects of plant adaptogens. III. Astragalus (Fabaceae). Central Eur J Immunol. 2011; 36: 104-107.

10. Liu MH, Li PL, Zeng X et al. Identification and Pharmacokinetics of Multiple Potential Bioactive Constituents after Oral Administration of Radix Astragali on Cyclophosphamide-Induced Immunosuppression in Balb/c Mice. Int J Mol Sci. 2015; 16: 5047-5071.

11. Ali M, Khan T, Fatima K et al. Selected hepatoprotective herbal medicines: Evidence from ethnomedicinal applications, animal models, and possible mechanism of actions. Phytother Res. 2018; 32: 199-215.

12. Gong P, Wang DN, Cui DD et al. Anti-aging function and molecular mechanism of Radix Astragali and Radix Astragali preparata via network pharmacology and PI3K/Akt signaling pathway. Phytomedicine. 2021; 84: 11.

13. Phu HT, Thuan DTB, Nguyen THD et al. Herbal Medicine for Slowing Aging and Aging-associated Conditions: Efficacy, Mechanisms and Safety. Current Vascular Pharmacology. 2020; 18: 369-393.

14. Li K, Li SY, Wang D et al. Extraction, Characterization, Antitumor and Immunological Activities of Hemicellulose Polysaccharide from Astragalus radix Herb Residue. Molecules. 2019; 24: 21.

15. Commission CP. Pharmacopoeia of the People's Republic of China. Beijing: China Medical Technology Publishing House; 2020.

16. Cheng XF, Zhang M, Adhikari B et al. Effect of Power Ultrasound and Pulsed Vacuum Treatments on the Dehydration Kinetics, Distribution, and Status of Water in Osmotically Dehydrated Strawberry: a Combined NMR and DSC Study. Food Bioprocess Technol. 2014; 7: 2782-2792.

17. Chen YN, Li M, Dharmasiri TSK et al. Novel ultrasonic-assisted vacuum drying technique for dehydrating garlic slices and predicting the quality properties by low field nuclear magnetic resonance. Food Chemistry. 2020; 306.

18. Wang L, Xu BG, Wei BX et al. Low frequency ultrasound pretreatment of carrot slices: Effect on the moisture migration and quality attributes by intermediate-wave infrared radiation drying. Ultrasonics Sonochemistry. 2018; 40: 619-628.

19. Song YK, Zang X, Kamal T et al. Real-time detection of water dynamics in abalone (Haliotis discus hannai Ino) during drying and rehydration processes assessed by LF-NMR and MRI. Dry Technol. 2018; 36: 72-83.

20. Ezeanaka MC, Nsor-Atindana J, Zhang M. Online Low-field Nuclear Magnetic Resonance (LF-NMR) and Magnetic Resonance Imaging (MRI) for Food Quality Optimization in Food Processing. Food Bioprocess Technol. 2019; 12: 1435-1451.

21. Cheng SS, Wang XH, Li RR et al. Influence of multiple freeze-thaw cycles on quality characteristics of beef semimembranous muscle: With emphasis on water status and distribution by LF-NMR and MRI. Meat Sci. 2019; 147: 44-52.

22. Li Y, Zhang K, Xiong H et al. Application Progress of Texture Analyzer in Pharmaceutical Preparation Research. Chinese Journal of Experimental Traditional Medical Formulae. 2020; 26: 226-234.

23. Thakor NJ, Sokhansanj S, Sosulski FW et al. Mass and dimensional changes of single canola kernels during drying. J Food Eng. 1999; 40: 153-160.

518 24. Wang G, Deng Y, Xu X et al. Optimization of air jet impingement drying of
519 okara using response surface methodology. Food Control. 2016; 59: 743-749.
520 25. Tunde-Akintunde TY. Mathematical modeling of sun and solar drying of chilli
521 pepper. Renewable Energy. 2011; 36: 2139-2145.
522 26. Azzouz S, Guizani A, Jomaa W et al. Moisture diffusivity and drying kinetic
523 equation of convective drying of grapes. J Food Eng. 2002; 55: 323-330.
524 27. Cui L, Chen YN, Li M et al. Detection of water variation in rosebuds during
525 hot-air drying by LF-NMR and MRI. Dry Technol. 2020; 38: 304-312.
526 28. Ismagilov ZR, Yashnik SA, Matveev AA et al. Characteristics of drying and
527 active component distribution in alumina monoliths using (HL)-H-1-NMR
528 imaging. Catalysis Today. 2005; 105: 484-491.
529 29. Heikkinen S, Alvila L, Pakkanen TT et al. NMR imaging and differential
530 scanning calorimetry study on drying of pine, birch, and reed pulps and their
531 mixtures. Journal of Applied Polymer Science. 2006; 100: 937-945.
532 30. Dinani ST, Havet M. The influence of voltage and air flow velocity of combined
533 convective-electrohydrodynamic drying system on the kinetics and energy
534 consumption of mushroom slices. Journal of Cleaner Production. 2015; 95: 203-
535 211.
536 31. Murthy TPK, Manohar B. Hot air drying characteristics of mango ginger:
537 Prediction of drying kinetics by mathematical modeling and artificial neural
538 network. Journal of Food Science and Technology-Mysore. 2014; 51: 3712-
539 3721.

32. Li M, Chen YN, Wang X et al. Determination of drying kinetics and quality changes of Panax quinquefolium L. dried in hot-blast air. LWT-Food Sci Technol. 2019; 116.

33. Nemeth K, Plumb GW, Berrin JG et al. Deglycosylation by small intestinal epithelial cell beta-glucosidases is a critical step in the absorption and metabolism of dietary flavonoid glycosides in humans. European Journal of Nutrition. 2003; 42: 29-42.

34. Hostetler GL, Riedl KM, Schwartz SJ. Effects of food formulation and thermal processing on flavones in celery and chamomile. Food Chemistry. 2013; 141: 1406-1411.

35. Xu BJ, Chang SKC. Total Phenolic, Phenolic Acid, Anthocyanin, Flavan-3-ol, and Flavonol Profiles and Antioxidant Properties of Pinto and Black Beans (Phaseolus vulgaris L.) as Affected by Thermal Processing. Journal of Agricultural and Food Chemistry. 2009; 57: 4754-4764.

36. An KJ, Wei L, Fu MQ et al. Effect of Carbonic Maceration (CM) on the Vacuum Microwave Drying of Chinese Ginger (Zingiber officinaleRoscoe) Slices: Drying Characteristic, Moisture Migration, Antioxidant Activity, and Microstructure. Food Bioprocess Technol. 2020; 13: 1661-1674.

37. Chen YN, Dong HJ, Li JK et al. Evaluation of a Nondestructive NMR and MRI Method for Monitoring the Drying Process of Gastrodia elata Blume. Molecules. 2019; 24.

38. Sekiyama Y, Horigane AK, Ono H et al. T-2 distribution of boiled dry spaghetti

562 measured by MRI and its internal structure observed by fluorescence
563 microscopy. Food Research International. 2012; 48: 374-379.
564 39. Kirtil E, Oztop MH. H-1 Nuclear Magnetic Resonance Relaxometry and
565 Magnetic Resonance Imaging and Applications in Food Science and Processing.
566 Food Engineering Reviews. 2016; 8: 1-22.
567 40. Sun YA, Zhang M, Mujumdar AS et al. Pulse-spouted microwave freeze drying
568 of raspberry: Control of moisture using ANN model aided by LF-NMR. J Food
569 Eng. 2021; 292.
570 41. Kadam SU, Tiwari BK, O'Donnell CP. 6 - Improved thermal processing for food
571 texture modification. Woodhead Publishing; 2015.
572 42. Waldron KW, Smith AC, Parr AJ et al. New approaches to understanding and
573 controlling cell separation in relation to fruit and vegetable texture. Trends in
574 Food Science & Technology. 1997; 8: 213-221.
575 43. Mina B, Jeevani V, Revathy S et al. Phytochemical and microscopical
576 investigations on Lawsonia inermis roots. International Journal of Current
577 Pharmaceutical Review and Research. 2012; 3: 54-59.
578

# Supplementary Files

This is a list of supplementary files associated with this preprint. Click to download.

- Table1.xlsx
- Table2.xlsx
- Table3.xlsx
- Table4.xlsx